Laser processing of SiC: From graphene-coated SiC particles to 3D graphene froths

CrossMark

Aspasia Antonelou [a,b], Vassileios Dracopoulos [a], Spyros N. Yannopoulos [a,*]

[a] Foundation for Research and Technology Hellas, Institute of Chemical Engineering Sciences (FORTH/ICE-HT), P.O. Box 1414, GR-26504 Rio-Patras, Greece
[b] Department of Materials Science, University of Patras, GR-26504 Rio-Patras, Greece

ARTICLE INFO

ABSTRACT

Production of graphene-based structures and composites can be achieved in a number of ways using predominantly chemical-vapor-deposition-based approaches and solution chemistry methods. The present work investigates the feasibility of infrared lasers in the controlled graphitization of micron-sized SiC particles. It is demonstrated that laser-mediated SiC decomposition can result in a manifold of graphene structures depending on the irradiation conditions. In particular, graphene formation, at nearly ambient conditions, can take place in various forms resulting in SiC particles covered by few-layer epitaxially grown films, and particles with a progressively increasing thickness of the graphitized layer, reaching eventually to free-standing 3D graphene froths at higher irradiation doses. Electron microscopies are used to determine the graphene layer features while Raman scattering identifies high-quality, strain-free graphene. Implications of graphene-coated particles and 3D porous graphene scaffolds to a variety of applications are briefly discussed. The present findings testify the potential of lasers toward the tailor-made preparation of high-quality graphene-based structures. The scalability and adaptability of lasers further support their prospect to develop reliable, reproducible, eco-friendly and cost-effective laser-assisted graphene production technologies.

1. Introduction

After almost one decade of systematic and intense fundamental graphene research it is generally agreed that graphene's superior physical properties (optical, electrical, and so on) are currently well understood [1–3]. Major experimental challenges are now related to the large-scale production of high-quality graphene and graphene-based structures, which is the prerequisite to evolve fundamental graphene science into viable technological applications [2,3].

Among the various graphene growth methods, the chemical vapor deposition (CVD) of hydrocarbons and epitaxial growth on the surface of transition metals, such as Ni or Cu, has been widely used for large area graphene growth. However, transfer of the graphene onto different substrates not only affects graphene's properties and performance, but also necessitates sample cleaning procedures to remove unwanted residues deposited during the transfer process. In addition, for particular applications, one is confronted with challenges such as growing graphene in various geometries (not simply as a 2D layer) and coating particles with graphene

layers to exploit nanocomposites' properties, etc. Obviously, traditional methods such as CVD cannot offer feasible solutions to such challenges. On the other hand, one of the most promising methods for large area, high quality graphene production is the thermal decomposition of SiC, which leads to the growth of epitaxial graphene (EG) [4–6] with high potential for applications in electronics and photonics/optoelectronics [2]. The EG growth is itself challenging with notable differences between EG growth on the Si- and C-terminated faces [7,8]. The predominant approach used to obtain EG on SiC is thermal annealing of SiC wafers either in high vacuum (at $T > 1500$ K) or under controlled Ar atmosphere (at $T > 1750$ K). However, even with this method, the use of strict chamber conditions (high temperature and/or high vacuum) and the lack of the possibility of *in situ* patterning (during growth) of graphene pose extra limitations toward fully exploiting graphene's assets to high-end applications.

The use of lasers for EG grow on SiC can offer a number of advantages as has been discussed elsewhere [9]. Among the various merits of this method, the most prominent one are perhaps the cost-effective and eco-friendly character of the approach – since not pre- or post-treatment with harmful chemicals is needed – and the feasibility offered by laser-assisted methods toward integration of graphene with existing technology platforms. However, there has been yet a limited number of investigations as regards the growth of EG using long-wavelength infrared, i.e. 10.6 μm [9], and ultra-violet, i.e. 248 nm [10], lasers, while the optimization of laser-grown graphene processes is still completely lacking.

Although in the vast majority of studies EG was grown onto single crystalline SiC wafers, interest has recently arisen in the growth of graphene-like structures on the surface of micro- and nano-sized SiC particles, as epigrammatically described below. Graphitized SiC particles (60–120 μm) prepared by high temperature thermal annealing were found to exhibit significant enhancement in photocatalytic activity under UV illumination, in comparison to the pristine SiC particles [11]. However, the Raman spectra reveal surface graphitization but did not demonstrate good quality graphene films [11]. Miranzo et al. [12] employing the spark plasma sintering technique, reported on the single-step process for *in situ* fabrication of graphene/SiC dense nanocomposites where good quality graphene films cover SiC particles. These nanocomposites, which were prepared by sintering (Joule heating) of submicron (0.5 μm) and nanometer (45–55 nm) sized particles, showed notable electrical and mechanical properties [12,13]. Apart from the thermal decomposition, another large class of nanostructures known as carbide-derived carbons (CDCs) emerge from chemical treatment (halogenation) of carbide precursors [14,15]. From the structural viewpoint, CDCs can be grown in a variety of forms including amorphous and nanocrystalline carbon, graphite, carbon nanotubes, carbon onions, nanodiamonds, and so on [14,15]. The synthesis parameters and the carbide precursor determine the structure of the CDCs and hence dictate the applications of such materials in tribology, gas storage and electrical energy storage.

In the current work we show that graphitization of SiC particles can proceed at a much faster time scale (few seconds) at practically ambient conditions using a CO_2 laser operating at 10.6 μm. Based on the irradiation conditions the processing of SiC powders can result in a variety of graphene morphologies from few-layer graphene-coated particles up to completely dilapidated particles with a froth-like texture where the Si content has been completely removed. Electron microscopies and Raman scattering are employed to characterize the morphology and quality of the graphene-like structures.

2. Experimental details

Two types of α-SiC powders with average particles sizes 2 μm (Alfa Aesar, 99.8%) and 20 μm (Alfa Aesar, >97%) were processed as received without any pre-treatment. The particles were either gently pressed to form a pellet into a 3 mm diameter/3 mm deep cylindrical hole drilled on an Aluminum block or dispersed into absolute ethanol and drop-casted on Au-coated Si substrates. The Aluminum block and/or the Si substrate were placed on a brass base which allows the Ar-purging into a funnel-type glass chamber as illustrated in the schematic of Fig. 1. The glass chamber enables the creation of an Ar rich atmosphere acting as a shielding gas above the SiC powder, in order to decrease the oxidation (burning) of the formed graphene structures.
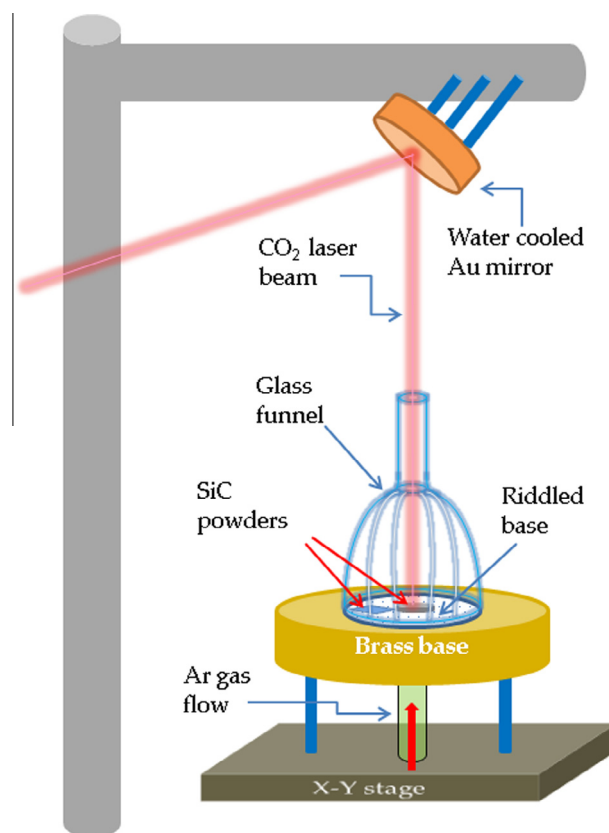
Fig. 1 – Schematic diagram of the illumination geometry. The CO_2 laser beam irradiates vertically the SiC powders placed either in the hole of an Aluminum block or in a Au-coated Si substrate. A funnel-like glass is used to create an Ar atmosphere shielding the irradiated material. (A color version of this figure can be viewed online.)

Laser irradiation takes place vertically, with the aid of an Au-coated, water-cooled mirror using a CO_2 laser (Synrad, Evolution Series; 240 W maximum power) operating at 10.6 μm with power levels between 15% and 30% of the maximum power. The merits of using this particular infrared wavelength for SiC decomposition have been described elsewhere in conjunction with the absorbance spectrum of SiC and its temperature dependence [9]. The SiC particles were subjected to gradually increasing irradiation-induced heating by raising the laser power to the desired level which was stopped by sudden shutting down the laser after few seconds. The 2 μm particles required increased levels of irradiation and longer heating times than the 20 μm particles to achieve graphitization. This finding may originate from the effect of particle size to the absorption and scattering of the laser radiation. In addition, the (sporadic) existence of graphitic remnants on the surfaces of the 20 μm sized pristine powders may also facilitate the absorption of the radiation.

Scanning electron microscopy (SEM) was carried out with a high resolution field-emission SEM (FE-SEM, Zeiss, SUPRA 35VP) operated at 5 kV. Transmission electron microscope (TEM) and high resolution TEM (HRTEM) images were taken on a JEOL JEM-2100 transmission electron microscope operated at 200 kV. The sample for the TEM analysis was prepared by a standard procedure; the laser-processed powders were dispersed in ethanol by ultrasonic waves and spread onto a carbon-coated copper grid (200 mesh). Raman spectra were recorded with the 514.5 nm laser line as the excitation source. The scattered light was analyzed by the T64000 (Jobin-Yvon) micro-Raman spectrometer at a spectral resolution of $\sim$1.5 cm^{-1}. A microscope objective with magnification 50× was used to focus the light onto a $\sim$2–3 μm spot. Low laser intensities were used (<0.1 mW on the sample) to avoid spectral changes due to heat-induced effects.

3. Results and discussion

3.1. Laser graphitization of 20 μm sized α-SiC particles

Representative FE-SEM images of the pristine and irradiated 20 μm SiC particles are shown in Fig. 2. Image 2(a) shows the pristine (untreated) SiC particles which exhibit smooth, well-faceted surfaces. The inset shows a magnified image of the surface of a pristine SiC particle; smaller SiC particles are attached to the large particle surfaces due to the preparation conditions. Irradiation dose increases in the series of the images 2(b)–(h). The images reveal that a progressive laser-induced processing of the particles surface takes place, which is systematically changing with the irradiation dose. Graphitization, in the form of an epitaxially grown film, is evident in image 2(b) as can be discerned from the variable contrast of the particle faces. In particular, a patchy morphology of epitaxial graphene is evident only for irradiated particles. The magnified image shown in 2(a) shows no signs of such contrast related to the formation of epitaxial graphene. The roughening of the surface, arising from the particle decomposition, is more apparent in image 2(c) where graphene flakes self-exfoliate, protruding out of the SiC particles' surface. The surface of the particles becomes increasingly irregular

at higher doses, as is illustrated in image 2(d), where grooves are formed at certain areas where Si evaporation is faster than the neighboring ones. The surface of the SiC particles becomes progressively rougher over a depth of several tens of nm as shown in images 2(e) and (f), where a sponge-like morphology emerges. Finally, prolonged irradiation leads to Si-depleted structures such as those shown in image 2(g), and in particular in 2(h), where a complete removal of the Si atoms over the whole volume of the particles results in particles with a froth-like, semi-transparent morphology. The inset in image 2(h) shows the graphene layers in higher magnification, where pores with dimensions of few tens of the nm are evident. The above mentioned show that a variable degree of graphitization of the surface of SiC particles is feasible upon irradiation over time scales of few tens of seconds (10–30 s).

Porous carbon structures resulting from complete Si removal have also been obtained by halogenation of β-SiC whiskers [15]. However, these halogenated-derived Si-depleted structures differ from those with the froth morphology shown in image 2(h). In the first case, the slow – and more controlled Si removal process – which takes place during the halogenation of β-SiC whiskers at 1200 °C leads to the so-called conformal carbide-to-carbon transformation where the original shape and volume of the carbide precursor are maintained [15]. However, the resulting halogenated-produced carbon structure is predominately amorphous with a very narrow pore size distribution peaked below 1 nm, while in the present case laser-produced carbon structures are highly crystalline – and in particular graphene-like – as evidenced from representative Raman spectra shown in Fig. 3. The Raman spectra, from (a) to (f), correspond to regions with gradually higher graphitization extent as shown in the FE-SEM images of Fig. 2 and in particular to images 2(b)–(g). Raman spectra (a)–(d) exhibit contributions from the second order Raman spectrum of SiC, in the range 1200–1900 cm^{-1}, which decreases systematically, indicating a progressive thickening of the graphene film in the order from (a) to (d).

Raman scattering is perhaps the most valuable (indirect) tool for exploring the quality of graphitic and graphene-like structures [16,17]. The quality of the grown graphene is usually evaluated through the relative intensity ratio of the D/G bands, which provides a measure of the defect concentration and crystallite size [18,19]. The defect-induced D-band (dispersive mode in the range 1300–1370 cm^{-1}) arises from the breathing mode of the sp^2 rings and becomes Raman active in the presence of defects, while the G-band ($\sim$1582 cm^{-1}), present to all sp^2 carbon networks, corresponds to the in-plane, doubly degenerate E_{2g} phonon at the center of the Brillouin zone. Firm criteria for estimating the number of graphene monolayers (MLs) have been established only for *mechanically cleaved graphene* films [20], based on the ratio of the 2D (second order of the D band originating from a double resonance process; historically called the G′ band [16]) over the G band. However, as has been pointed out elsewhere [8], comparing a more extensive set of EG Raman spectra, these criteria could be misleading for the estimation of the number of MLs in epitaxial graphene. Besides, combinations of the D, G, and 2D peak parameters are used to provide information concerning the layer stacking order (2D band shape, i.e. single
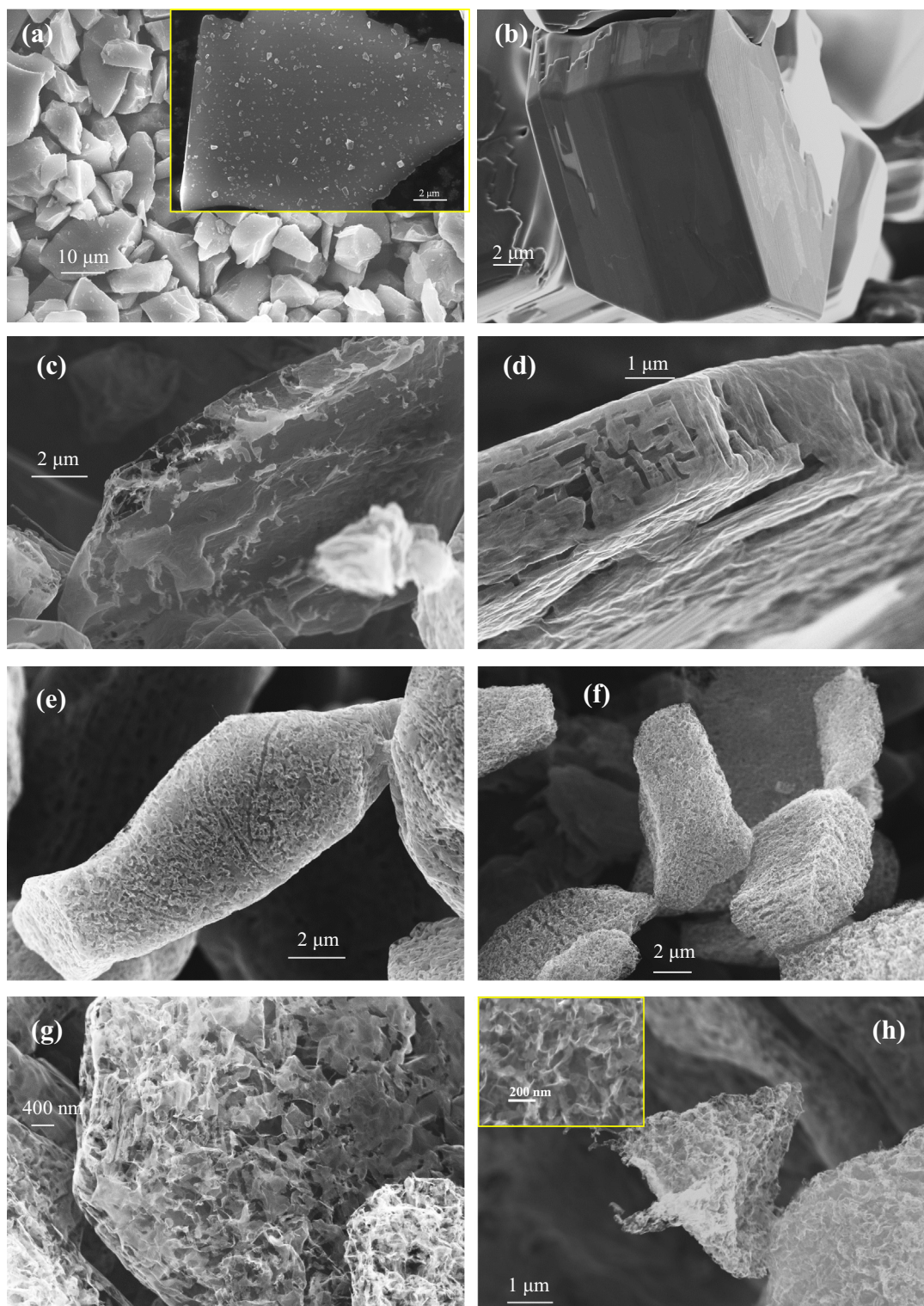
Fig. 2 – Typical FE-SEM images of laser-processed SiC particles (20 μm). From (a) to (h) images correspond to structures subjected to progressively higher dose. (A color version of this figure can be viewed online.)

or multiple lines) and mechanical stresses of the graphene film (G band shift; shape and Raman shift of 2D band). Given the above context, the Raman spectra of Fig. 3 provide the following information for laser-mediated graphene structures on SiC surfaces.

(i) The D band intensity is much lower than that of the G band in all cases, which together with the narrowness of the G band ($\sim$21 cm^{-1}), comparable to the FWHH of the G band in epitaxial graphene [8], reveals a very low defect concentration and hence a high crystallinity
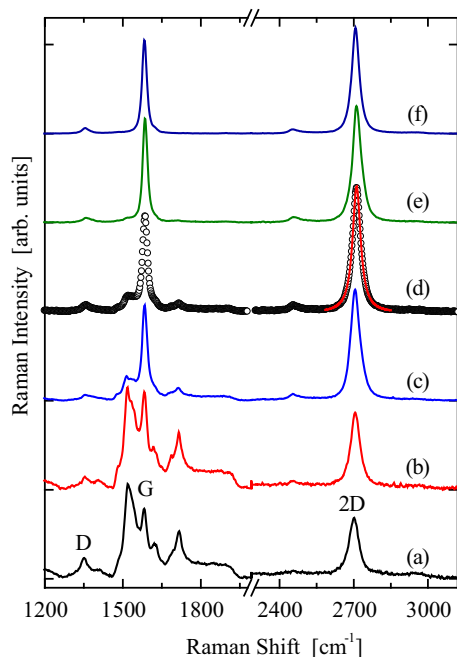
Fig. 3 – Representative Stokes-side Raman spectra of laser-processed SiC particles (20 μm). Their intensities have been normalized to unity (for the more intense band) and their baselines have been off-set for clarity. The 2D band of spectrum (d) has been fitted by a single Lorentzian line shown by the solid line passing through the data points. The Raman spectra, from (a) to (f), roughly correspond to specimen regions from where the FE-SEM images 2(b) to (g) were recorded. (A color version of this figure can be viewed online.)

of the graphene-like structures. An estimation of the graphene crystallites size results in a size of ca. 330 nm.

(ii) For all spectra shown in Fig. 3 the intensity (area) ratio of the G and D bands is in the range $1.5 < I^{2D}/I^G < 2.0$, demonstrating that the grown carbon structures are graphene-like, rather than amorphous/nanocrystalline carbon or graphite. Amorphous/nanocrystalline carbon exhibits characteristic weak, broad bands in the 2D band frequency while graphite shows a characteristic double 2D band peak with a low energy shoulder [16,17].

(iii) The 2D band is in all cases a narrow, single Lorentzian peak as is seen in a representative fit example shown in Fig. 3 for spectrum (d). The full-width at half height (FWHH) of the 2D band is $\Gamma(2D) \approx 36$ cm^{-1} which is even narrower than that of epitaxial graphene [7,8]. It is worth mentioning that even for monolayer epitaxial graphene grown on SiC(0001) the 2D band FWHH is of the same magnitude, i.e. 36 ± 2 [21], as that reported here for the SiC particles.

(iv) The frequency of the G and 2D bands are highly insensitive to the degree of graphitization of the SiC particles. Apart from spectrum (a) in Fig. 3, where $\omega(2D) \approx 2702$ cm^{-1}, the frequency of the 2D band for all other cases is rather constant with $\omega(2D) \approx 2710 \pm 3$ cm^{-1}. This finding surprisingly indicates a very good

uniformity of the strain distribution even if compared with monolayer EG in SiC. The latter is usually characterized by large variations of the 2D band energy, i.e. $2690 < \omega(2D) < 2735$ cm^{-1} for 532 nm laser excitation [8], and $2717 < \omega(2D) < 2737$ cm^{-1} for 482.5 nm laser excitation [21]. The present insensitivity of the $\omega(2D)$ variation is comparable to that measured in laser-grown EG on SiC(000$\bar{1}$) [9], suggesting that the ultrafast heating and cooling rates imposed by the laser treatment of SiC is presumably the origin of enhanced strain homogeneity in the graphene films. The G band frequency also shows very small fluctuations, being situated in the spectral range $\omega(G) \approx 1583 \pm 1$ cm^{-1} indicating practically absence of strain in the graphene films.

(v) The spectral shape of the 2D band demonstrates that the laser-assisted grown carbon on the SiC particles surface acquires a graphene-like configuration. Structures with increased interlayer spacing, up to 0.35 nm, were found in carbide-derived carbons prepared by halogenation, which were assigned to turbostratic graphite [22]. However, in the present case, the assignment of the obtained carbon structures to turbostratic graphite may be improper as the latter is characterized by small domain size, which at best reaches ~100 nm [23]. Therefore, based on our Raman spectra, the graphene-like structures obtained here bear a close resemblance to multilayer graphene growing on the C-face of SiC [24]. However, the high I^{2D}/I^G and the narrowness of the 2D band imply that some contribution in the Raman spectra of free-standing, exfoliated graphene monolayers is likely, especially for the structures with severe Si depletion. The increased interlayer spacing between graphene planes brings about weakening of the interlayer interactions which further induces electronic decoupling of the layers, as is also the case of non-Bernal stacked, multi-layer graphene grown on the C-face of SiC [23–25]. The appearance of Dirac-like electronic states in multilayer C-face, rotationally faulted graphene, is the origin of enhanced transport properties, which are comparable to those of the single layer graphene [23–25].

Representative HRTEM images of laser-processed, 20 μm sized, SiC particles are shown in Fig. 4. These images correspond to irradiation conditions that lead to SiC particle morphologies similar to those revealed by the SEM images shown in Fig. 2(e)–(h). The images confirm the decomposition of the SiC lattice and the subsequent formation of graphene layers at the surface of the irradiated SiC particles. In the vast majority of the particles explored, graphene layers appear to maintain their integrity; therefore, regions of amorphous carbon are largely absent. In this sense, HRTEM corroborates the findings of Raman spectroscopy of an appreciably low defect density graphene-like phase. For all studied cases, the graphene interlayer distance was measured to be considerably larger than that of the highly-oriented pyrolytic or planar graphite, i.e. 0.334 nm, which points to an arrangement of electronically decoupled graphene layers; hence, confirming again the conclusions drawn by the Raman analysis of the 2D band shape. Measured interlayer distances of the graphene layers

shown in Fig. 4 vary in the interval 0.36–0.40 nm. The inset in image 4(C) displays the power spectrum of the resulting Fast Fourier Transform (FFT) of this particular arrangement of graphene layers. The disordered nature of the layers is the origin of the diffuse 002 diffraction spots corresponding to the interlayer distance d_{002}. An estimation of the interlayer spacing results in $d_{002} = 0.399$ nm, which is in agreement with the 0.403 nm value determined by the HRTEM image. HRTEM images illustrate in certain cases the formation of ribbons of few-layer graphene sheets, which has also been observed in CDCs prepared by chemical treatment (halogenation) [21]. Notably, the amorphous carbon content, in those chemically prepared CDCs [21], is appreciably higher than that obtain in the laser treated SiC particles.

3.2.   Laser graphitization of 2 μm sized α-SiC particles

The results of the irradiation of 2 μm sized α-SiC particles were found to be qualitatively different than those of the larger (20 μm) particles. In general, higher irradiation dose – almost twice as that used for the large particles – was needed to commence graphitization to the 2 μm SiC particles. This effect can possibly be related to the enhanced diffraction and interference effects for the 2 μm SiC particles due to the proximity between the particle size and the laser wavelength. We expect that for submicron particles, such effects will not play dominant role and in particular for nanometer-scale SiC particle graphitization will be feasible due to the contrasting lengths scales between particle size and CO_2 laser wavelength. The use of near-to-mid-infrared lasers of different wavelengths could be an alternative to overcome the above problem. However, the scarcity of such lasers in this energy range and the difference in the absorption coefficient of SiC at wavelengths lower than 10.6 μm are factors to be considered for a thorough understanding of SiC graphitization with different lasers.

Typical FE-SEM images are presented in Fig. 5. These images reveal that the morphology of the irradiated SiC particles is more homogeneous at various irradiation zones than that of the larger particles. The main outcome of the laser-induced Si removal is the smoothening of the SiC particles' surface and the formation of, mostly, epitaxial-like carbon material on the surfaces, as can be seen in images 5(d) and (e). Notably, no appreciable in-depth graphitization of the 2 μm SiC particles was possible. However, in rare cases, particles covered by thick carbon layers, see e.g. image 5(f) were observed.

The structure of the graphitized areas was evaluated using Raman scattering. Fig. 6 shows representative Raman spectra recorded from various regions of the irradiated samples. Based on the criteria discussed above, the Raman spectra can be interpreted as showing also in this case the growth of graphene-like carbon structures. However, the graphene quality is not as good as that for the larger (20 μm) SiC particles. The I^D/I^G band intensity ratio is larger in the case of the 2 μm particles revealing a rather small crystallite size, not larger than ∼50 nm. The 2D band is mostly a single Lorentzian peak with a FWHH in the range 50–60 cm^{-1}, i.e. substantially broader than the 2D band in the large (20 μm) SiC particles; albeit comparable with the FWHH of epitaxial graphene on the C-face of SiC [8]. This effect is possibly associated to a larger degree of disorder in terms of random orientations between graphene layers, which can cause relaxation of the double-resonance Raman selection rules [16]. The 2D band
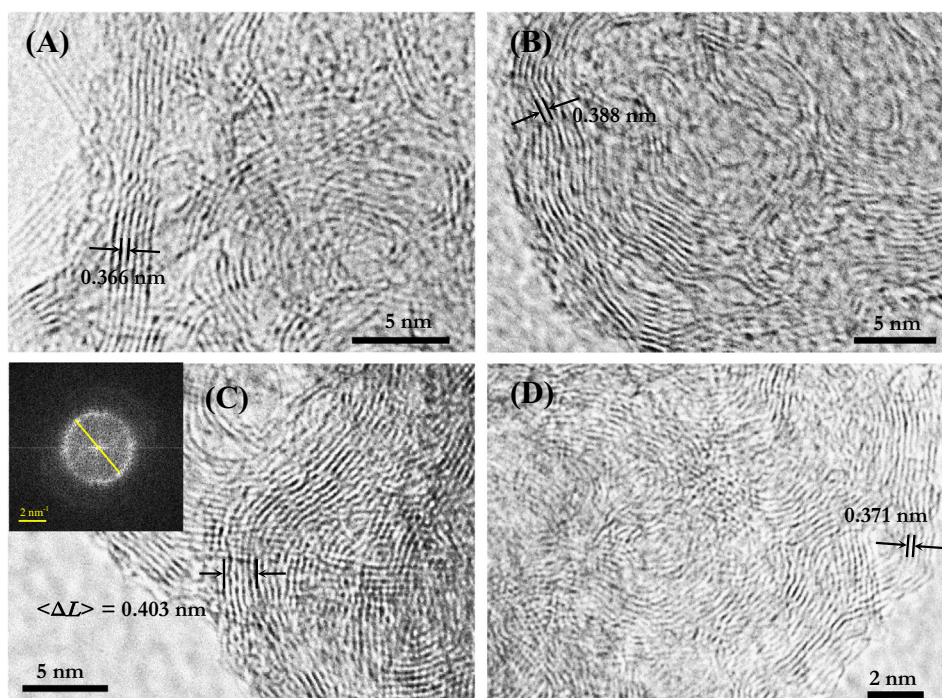
Fig. 4 – Typical HRTEM images of laser-processed SiC particles (20 μm). Characteristic interlayer spacing is shown, revealing an interlayer distance in all cases appreciably larger than that of graphite. The mean interlayer spacing for several layers is shown in (C). The inset shows the FFT of the image. (A color version of this figure can be viewed online.)

energy is located in the interval $\omega(2D) = 2710 \pm 1$ cm^{-1} for the thick graphene films (spectra c,d,e in Fig. 6) and $\omega(2D) = 2720 \pm 3$ cm^{-1} for the partially graphitized particles, implying an increased level of compressive strain exerted to the graphene layers by the substrate. In addition to compressive strain, charge doping originating from the substrate – or doping emerging from ambient oxygen/water – has also been considered to explain the blue-shift of the 2D band [16,17]. However, given that all graphitized samples were prepared under the same conditions, the blue-shift of the 2D band in the case of the partially graphitized sample (Fig. 6, spectra a,b) is not likely to arise from doping effects, and hence strain effects seem as a more probable cause of this effect.

3.3. Implications of graphene-coated SiC particles and non-planar graphene structures

The main outcome of the current work, i.e. the formation of either graphene-coated SiC particles or non-planar graphene structures in the form of porous assemblies or froths presents implications for a variety of emerging technologies and applications. The SiC particles coated by few-layer graphene films are considered for applications in macro- and nano-electromechanical systems owing to their very high electrical conductivity, which can reach to 100 S m^{-1} for spark plasma sintered nanosized SiC particles [12]. This amounts to about ten orders

of magnitude enhancement of the electrical conductivity in comparison to the non-graphitized SiC particles [12]. Graphene coated SiC particles were also recently prepared at high temperature (1600–2200 °C) in a way simulating the encapsulation of fissionable material and fission products by layers of carbon and SiC (fuel particles) in high temperature reactors, and their mechanical properties were studied in detail [26]. Further, owing to their electro-conductive properties, graphene-coated nanocomposites exhibit strong potential to be used as electromagnetic interference materials with high shielding effectiveness for THz electromagnetic waves [27].

On the other side, there has recently been strong interest in *non-planar* graphene-based structures especially in view of their high surface area and pore volume. Various morphologies such as crumpled graphene [28], graphene nanomesh (reduced graphene oxide retaining in-plane pores) [29,30] and graphene foam [31,32] have been systematically explored since they also exhibit high thermal stability and mechanical strength. Graphene structures that combine the above properties are suitable for a number of applications including sensors, energy storage, gas separation, gas storage, fuel cells, supercapacitors, Li-ion batteries, etc. In their vast majority, these porous graphene-based materials are produced by reduced graphene oxide. Although the production of graphene oxide can be scalable to large volumes, its viability in applications is still limited for the following reasons.
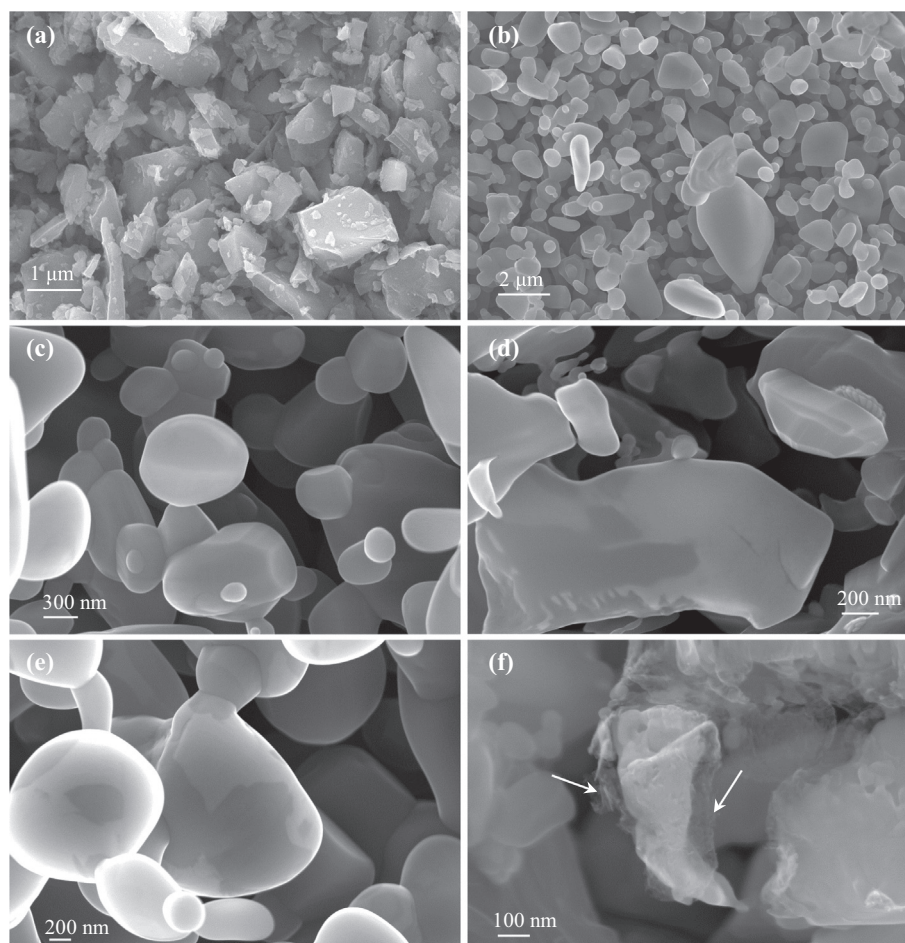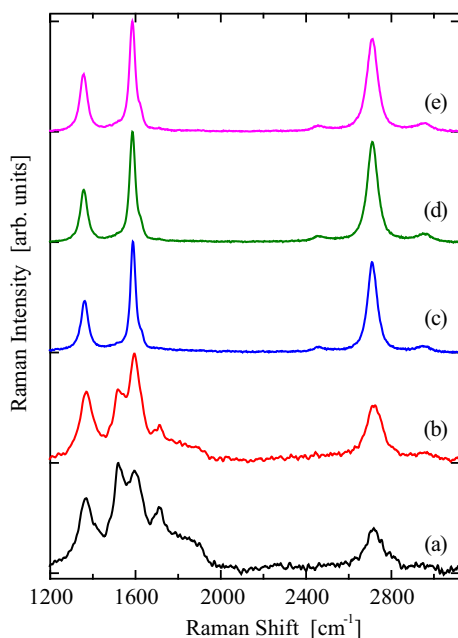

Fig. 5 – Typical FE-SEM images of laser-processed SiC particles (2 μm).

Fig. 6 – Representative Stokes-side Raman spectra of laser-processed SiC particles (2 μm). Their intensities have been normalized to unity (for the more intense band) and their baselines have been off-set for clarity. (A color version of this figure can be viewed online.)

graphitization can take place under various morphologies. These morphologies can range from epitaxial-like growth of few layer graphene (surface graphitization) up to highly porous graphene-like structures (froth morphology). Such structures emerge from the laser-assisted graphitization of large (20 μm) α-SiC particles, while only surface graphitization takes place by irradiating small (2 μm) particles. Laser-induced graphitization is evidently a versatile and adaptable technique for the preparation of carbide-derived carbons from inorganic precursors. Scalability of laser-assisted CDCs production to large scale appears realistic in view of the high rate of laser processing (short time decomposition) and the fact that strict sample-environment conditions (high vacuum, high temperature) are not necessary.

Acknowledgements

Graphene oxide is a material with inferior properties (e.g. electrical, optical, specific capacitance, energy density and power density) compared to graphene and thus can be used for less-demanding applications. Its production involves elaborate chemistry approaches. Graphene oxide sheets in liquid media have the tendency to interact by van der Waals forces toward agglomeration/restacking which can lead to the reestablishment of graphitic structures, thus losing their high specific surface area.

The main advantage of the laser-induced decomposition of SiC particles into 3D porous graphene networks, apart from being fast and cost-effective, is that no pre- or post-treatment is needed with hazardous for the environment chemicals. Further, the solid 3D graphene scaffolds grown by the laser method provide solid networks overcoming the drawbacks of solution approaches. As regards porosity, CDCs produced by SiC halogenation are characterized by microporous (<2 nm) structures [15], where the halogenation temperature controls finely the pore size distribution. Crumpled graphene is characterized by porosity in the mesoporous to the macroporous scale [28], while graphene foam assumes a macroporous structure [31]. The Si-depleted graphene-like 3D froths, shown in Fig. 2(g) and (h), can be considered as mesoporous structures characterized by pores of the order of few tens of nm's. However, optimization of the irradiation parameters might offer tuneability to the porosity of the laser-mediated grown CDCs.

4. Concluding remarks

In summary, the results presented here demonstrate that depending on the SiC particle size and irradiation details,

REFERENCES

[1] Novoselov KS, Fal'ko VI, Colombo L, Gellert PR, Schwab MG, Kim K. A roadmap for graphene. Nature 2012;490:192–200. http://dx.doi.org/10.1038/nature11458.

[2] Avouris P, Dimitrakopoulos C. Graphene: synthesis and applications. Mater Today 2012;15:86–97. http://dx.doi.org/10.1016/S1369-7021(12)70044-5.

[3] Raza H, editor. Graphene nanoelectronics. Berlin, Heidelberg: Springer, Berlin Heidelberg; 2012. http://dx.doi.org/10.1007/978-3-642-22984-8.

[4] Seyller T. Epitaxial graphene on SiC(0001). In: Raza H, editor. Graphene nanoelectron. Berlin, Heidelberg: Springer Berlin Heidelberg; 2012. p. 135–55. http://dx.doi.org/10.1007/978-3-642-22984-8.

[5] Camara N, Rius G, Huntzinger J-R, Tiberj A, Mestres N, Godignon P, et al. Selective epitaxial growth of graphene on SiC. Appl Phys Lett 2008;93:123503. http://dx.doi.org/10.1063/1.2988645.

[6] De Heer WA, Berger C, Ruan M, Sprinkle M, Li X, Hu Y, et al. Large area and structured epitaxial graphene produced by confinement controlled sublimation of silicon carbide. Proc Natl Acad Sci USA 2011;108:16900–5. http://dx.doi.org/10.1073/pnas.1105113108.

[7] Cambaz ZG, Yushin G, Osswald S, Mochalin V, Gogotsi Y. Noncatalytic synthesis of carbon nanotubes, graphene and graphite on SiC. Carbon N Y 2008;46:841–9. http://dx.doi.org/10.1016/j.carbon.2008.02.013.

[8] Giusca CE, Spencer SJ, Shard AG, Yakimova R, Kazakova O. Exploring graphene formation on the C-terminated face of SiC by structural, chemical and electrical methods. Carbon N Y 2014;69:221–9. http://dx.doi.org/10.1016/j.carbon.2013.12.018.

[9] Yannopoulos SN, Siokou A, Nasikas NK, Dracopoulos V, Ravani F, Papatheodorou GN. CO₂-laser-induced growth of epitaxial graphene on 6H-SiC(0001). Adv Funct Mater 2012;22:113–20. http://dx.doi.org/10.1002/adfm.201101413.

[10] Lee S, Toney MF, Ko W, Randel JC, Jung HJ, Munakata K, et al. Laser-synthesized epitaxial graphene. ACS Nano 2010;12:7524–30.

[11] Zhu K, Guo L, Lin J, Hao W, Shang J, Jia Y, et al. Graphene covered SiC powder as advanced photocatalytic material. Appl Phys Lett 2012;100:023113. http://dx.doi.org/10.1063/1.3676042.

[12] Miranzo P, Ramírez C, Román-Manso B, Garzón L, Gutiérrez HR, Terrones M, et al. In situ processing of electrically conducting graphene/SiC nanocomposites. J Eur Ceram Soc 2013;33:1665–74. http://dx.doi.org/10.1016/j.jeurceramsoc.2013.01.021.

[13] Román-Manso B, Sánchez-González E, Ortiz AL, Belmonte M, Isabel Osendi M, Miranzo P. Contact-mechanical properties at pre-creep temperatures of fine-grained graphene/SiC composites prepared in situ by spark-plasma sintering. J Eur Ceram Soc 2014;34:1433–8. http://dx.doi.org/10.1016/j.jeurceramsoc.2013.11.00.

[14] Yushin G, Nikitin A, Gogotsi G. Carbide-derived carbon. In: Gogotsi Y, Volker P, editors. Carbon nanomater. CRC Press; 2006. p. 211–54.

[15] Presser V, Heon M, Gogotsi Y. Carbide-derived carbons – from porous networks to nanotubes and graphene. Adv Funct Mater 2011;21:810–33. http://dx.doi.org/10.1002/adfm.201002094.

[16] Malard LM, Pimenta MA, Dresselhaus G, Dresselhaus MS. Raman spectroscopy in graphene. Phys Rep 2009;473:51–87. http://dx.doi.org/10.1016/j.physrep.2009.02.003.

[17] Ferrari AC, Basko DM. Raman spectroscopy as a versatile tool for studying the properties of graphene. Nat Nanotechnol 2013;8:235–46. http://dx.doi.org/10.1038/nnano.2013.46.

[18] Tuinstra F. Raman spectrum of graphite. J Chem Phys 1970;53:1126. http://dx.doi.org/10.1063/1.1674108.

[19] Cançado LG, Takai K, Enoki T, Endo M, Kim YA, Mizusaki H, et al. General equation for the determination of the crystallite size L[sub a] of nanographite by Raman spectroscopy. Appl Phys Lett 2006;88:163106. http://dx.doi.org/10.1063/1.219605.

[20] Ferrari AC, Meyer JC, Scardaci V, Casiraghi C, Lazzeri M, Mauri F, et al. Raman spectrum of graphene and graphene layers. Phys Rev Lett 2006;97:187401. http://dx.doi.org/10.1103/PhysRevLett. 97.187401.

[21] Oliveira MH, Schumann T, Fromm F, Koch R, Ostler M, Ramsteiner M, et al. Formation of high-quality quasi-free-standing bilayer graphene on SiC(0001) by oxygen intercalation upon annealing in air. Carbon N Y 2013;52:83–9. http://dx.doi.org/10.1016/j.carbon.2012.09.008.

[22] Welz S, McNallan MJ, Gogotsi Y. Carbon structures in silicon carbide derived carbon. J Mater Process Technol 2006;179:11–22. http://dx.doi.org/10.1016/j.jmatprotec.2006.03.103.

[23] Hass J, Varchon F, Millán-Otoya J, Sprinkle M, Sharma N, de Heer W, et al. Why multilayer graphene on 4H-SiC(0001) behaves like a single sheet of graphene. Phys Rev Lett 2008;100:125504. http://dx.doi.org/10.1103/PhysRevLett. 100.125504.

[24] Faugeras C, Nerrière A, Potemski M, Mahmood A, Dujardin E, Berger C, et al. Few-layer graphene on SiC, pyrolitic graphite, and graphene: a Raman scattering study. Appl Phys Lett 2008;92:011914. http://dx.doi.org/10.1063/1.282897.

[25] Pankratov O, Hensel S, Bockstedte M. Electron spectrum of epitaxial graphene monolayers. Phys Rev B 2010;82:121416. http://dx.doi.org/10.1103/PhysRevB.82.121416.

[26] Rohbeck N, Xiao P. Effects of thermal treatment on the mechanical integrity of silicon carbide in HTR fuel up to 2200 °C. J Nucl Mater 2014;451:168–78. http://dx.doi.org/10.1016/j.jnucmat.2014.03.039.

[27] Liu L, Das A, Megaridis CM. Terahertz shielding of carbon nanomaterials and their composites – a review and applications. Carbon N Y 2014;69:1–16. http://dx.doi.org/10.1016/j.carbon.2013.12.021.

[28] Luo J, Jang HD, Sun T, Xiao L, He Z, Katsoulidis AP, et al. Compression and aggregation-resistant particles of crumpled soft sheets. ACS Nano 2011;5:8943–9. http://dx.doi.org/10.1021/nn203115u.

[29] Bai J, Zhong X, Jiang S, Huang Y, Duan X. Graphene nanomesh. Nat Nanotechnol 2010;5:190–4. http://dx.doi.org/10.1038/nnano.2010.8.

[30] Akhavan O. Graphene nanomesh by ZnO nanorod photocatalysts. ACS Nano 2010;4:4174–80. http://dx.doi.org/10.1021/nn1007429.

[31] Xu Y, Sheng K, Li C, Shi G. Self-assembled graphene hydrogel via a one-step hydrothermal process. ACS Nano 2010;4:4324–30. http://dx.doi.org/10.1021/nn101187z.

[32] Chen Z, Ren W, Gao L, Liu B, Pei S, Cheng H-M. Three-dimensional flexible and conductive interconnected graphene networks grown by chemical vapour deposition. Nat Mater 2011;10:424–8. http://dx.doi.org/10.1038/nmat3001.